Monthly Notices of the ROYAL ASTRONOMICAL SOCIETY
MNRAS Advance Access published January 7, 2013
MNRAS (2013) doi:10.1093/mnras/sts555

An examination of the spectral variability in NGC 1365 with *Suzaku*

L. W. Brenneman,[1⋆] G. Risaliti,[1,2] M. Elvis[1] and E. Nardini[1]

[1]*Harvard-Smithsonian Center for Astrophysics, 60 Garden St, Cambridge, MA 02138, USA*
[2]*INAF – Osservatorio Astrofisico di Arcetri, Largo E. Fermi 5, I-50125 Firenze, Italy*

Accepted 2012 December 3. Received 2012 November 8; in original form 2012 September 24

ABSTRACT

We present jointly analysed data from three deep *Suzaku* observations of NGC 1365. These high-signal-to-noise spectra enable us to examine the nature of this variable, obscured active galactic nucleus (AGN) in unprecedented detail on time-scales ranging from hours to years. We find that in addition to the power-law continuum and absorption from ionized gas seen in most AGN, inner disc reflection and variable absorption from neutral gas within the broad emission line region are both necessary components in all three observations. We confirm the clumpy nature of the cold absorbing gas, though we note that occultations of the inner disc and corona are much more pronounced in the high-flux state (2008) than in the low-flux state (2010) of the source. The onset and duration of the 'dips' in the X-ray light curve in 2010 are both significantly longer than in 2008, however, indicating that either the distance to the gas from the black hole is larger or the nature of the gas has changed between epochs. We also note significant variations in the power-law flux over time-scales similar to the cold absorber, both within and between the three observations. The warm absorber does not vary significantly within observations, but does show variations in column density of a factor of $\geq$10 on time-scales of $\leq$2 weeks that seem unrelated to the changes in the continuum, reflection or cold absorber. By assuming a uniform iron abundance for the reflection and absorption, we have also established that Fe/solar $= 3.5^{+0.3}_{-0.1}$ is sufficient to model the broad-band spectrum without invoking an additional partial-covering absorber. Such a measurement is consistent with previous published constraints from the 2008 *Suzaku* observation alone, and with results from other Seyfert AGN in the literature.

Key words: accretion, accretion discs – galaxies: active – galaxies: individual: NGC 1365 – X-rays: galaxies.

1 INTRODUCTION

In recent years, evidence has been mounting that the putative 'dusty torus' of active galactic nuclei (AGN) unification schemes (Antonucci 1993; Urry & Padovani 1995) is not a homogeneous structure. X-ray studies of several Seyfert AGN have demonstrated significant variability in the column density and/or covering fraction of the cold absorbing gas at typical radii of $r \geq 10\,000\,r_{\rm g}$ from the supermassive black hole (Risaliti, Elvis & Nicastro 2002; Risaliti et al. 2005b, 2010, 2011b). Physical interpretations for this inhomogeneity include a patchy structure for the torus itself (e.g., Turner et al. 2011), a system of comet-shaped, approximately neutral gas clouds orbiting the black hole at Keplerian velocities within the broad emission line region (BELR; e.g. Maiolino et al. 2010), or perhaps a dust-driven wind beyond the dust sublimation radius powered by radiation pressure from the disc emission (Hryniewicz & Czerny 2012).

For black holes accreting at even a modest rate ($L/L_{\rm Edd} \geq 0.01$, as per Fender, Gallo & Russell 2010), the accretion flow is expected to remain optically thick and only moderately ionized down to at, or very near, the innermost stable circular orbit (ISCO) in the disc (Reynolds & Fabian 2008). As such, if the standard picture of AGN X-ray emission is correct (i.e. coronal Compton scattering of the thermal disc photons, producing both the continuum power law and reflection spectrum from this scattered power-law emission reprocessed by the inner disc; e.g. Reynolds & Nowak 2003; Miller 2007), we should expect to see inner disc reflection features in any actively accreting AGN in which our line of sight to the inner disc is not completely obscured.[1] The most prominent example of these reflection features is the relativistically broadened Fe Kα line at

⋆ E-mail: lbrenneman@head.cfa.harvard.edu

[1] Note, however, that not all type 1 AGN that meet this requirement do show such features: X-ray surveys of hundreds of bright, nearby type 1 AGN indicate that only ∼40 per cent have broad Fe Kα lines, as per Nandra et al. (2007) and de La Calle Pérez et al. (2010), while even detailed, multi-epoch examinations of single AGN show potential evidence for an ephemeral presence of broad Fe Kα (Brenneman et al. 2012).

6.4 keV. This broad emission line was first detected in the Seyfert 1 AGN MCG-6-30-15 with *ASCA*, as reported by Tanaka et al. (1995), and has been confirmed by several successive missions with higher spectral resolution, e.g. *XMM–Newton* (Fabian et al. 2002) and *Suzaku* (Miniutti et al. 2007; Chiang & Fabian 2011).

If we look through a patchy/cloudy cold absorbing medium (even one that is Compton thick), we may view the broad Fe Kα line from the innermost accretion disc only intermittently. This opens up a new window of opportunity in the search for signatures of relativistic effects in AGN: an obscuring cloud covers/uncovers different parts of the accretion disc at different times, directly probing the nature of the disc emission. In particular, the combination of gravitational redshift and relativistic Doppler boosting should imply strong differences between the spectral appearance of the receding and approaching parts of an inclined, thin disc. For an 'eclipse' event of sufficient length, column density and contrast, and with enough signal-to-noise ratio (S/N), it is possible to obtain time-resolved spectra of the eclipse as different chords of the disc are covered/uncovered (Risaliti et al. 2011a). Examining the variation of the continuum and broad Fe Kα profile during such an event would yield definitive proof/disproof of the origin of the Fe Kα line as an inner disc reflection feature. It would also provide important constraints on the size of the inner disc/corona system and the physical properties and location of the eclipsing cloud. Finally, it would enable us to perform tomography of the inner accretion disc for the first time, tracing its physical properties as a function of radius.

In this paper, we report on three *Suzaku* observations of the Seyfert 1.8 galaxy NGC 1365 ($z = 0.005\,47$[2]). NGC 1365 is the first and most studied case of a patchy/cloudy cold absorbing medium ($N_{\rm H} \sim 10^{23}$–10^{24} cm^{-2}) occulting the inner accretion disc/corona system with a duty cycle of ∼50 per cent (Risaliti et al. 2002, 2005b, 2007, 2009b,c, 2010; Maiolino et al. 2010). Mass estimates for the supermassive black hole range from $M_{\rm BH} \sim 2 \times 10^6$ to 1×10^8 M$_\odot$ (Risaliti et al. 2009b and references therein), with a moderate Eddington ratio which is correspondingly uncertain [$L/L_{\rm Edd} \sim 0.02$–0.12, based on bolometric luminosities given in Vasudevan et al. (2010) and the masses quoted above]. In addition to its varying cold absorber and continuously seen broad Fe Kα line, *XMM–Newton* observations have revealed the presence of an ionized absorbing wind, manifesting as blueshifted absorption lines of Fe XXV and Fe XXVI from 6.7 to 8.3 keV. This wind varies in outflow velocity over weeks-to-months-long time-scales (Risaliti et al. 2005a). Hosted in a barred spiral galaxy of type SB(s)b (de Vaucouleurs et al. 1991), NGC 1365 also contains significant extended X-ray emission from a circumnuclear starburst, as imaged by *Chandra* (Wang et al. 2009). This emission dominates the X-ray spectrum below ∼2 keV, while the spectrum above ∼3 keV is dominated by the AGN itself.

The first *Suzaku* observation, taken in 2008, is described in detail in Risaliti et al. (2009a), Maiolino et al. (2010) and Walton, Reis & Fabian (2010). We re-examine its spectral and timing properties in the context of our two 2010 observations in order to assess the variability of the various spectral components of this AGN on time-scales ranging from hours to years. Our goal is to determine whether eclipses of the inner disc/corona by cold gas take place during our new observations, and to use these events to probe the structure of the nucleus and the nature of the inner accretion flow in NGC 1365. We describe our observations and data reduction in Section 2, our timing analysis in Section 3, and our time-averaged and time-resolved spectral analysis in Section 4. Discussions of our results and our conclusions are presented in Sections 5 and 6, respectively. Throughout the paper, we assume cosmological parameters of $H_0 = 70\,{\rm km\,s^{-1}\ Mpc^{-1}}$, $q_0 = 0$ and $\Lambda_0 = 0.73$.

[2] NED average redshift; http://ned.ipac.caltech.edu

2 OBSERVATIONS AND DATA REDUCTION

Suzaku (Mitsuda 2007) has observed NGC 1365 quasi-continuously on three occasions: 2008 January (160 ks), 2010 June (150 ks; 2010a) and 2010 July (300 ks; 2010b). The 2008 observation has been discussed at length by Risaliti et al. (2009a), Maiolino et al. (2010) and Walton et al. (2010), so its data reduction will not be detailed here, other than to say that we followed the reduction steps taken by Maiolino and Walton, but included the latest calibration updates. Here we focus on the reduction of the two 2010 observations, which were observed two weeks apart in a single campaign to search for the putative eclipses of the inner accretion disc that have been noted in previous observations of NGC 1365 (Risaliti et al. 2005b, 2007, 2009b,c; Maiolino et al. 2010).

2010a took place from June 27 to 30, while 2010b extended from July 15 to 22. In both instances the telescope was trained on NGC 1365 in the X-ray Imaging Spectrometer (XIS) nominal pointing position. The data from the three operational XIS instruments (XIS 0, XIS 1 and XIS 3; Koyama 2007) were reprocessed using the `xispi` script in accordance with the *Suzaku* ABC Guide[3] along with the latest version of the CALDB (as of 2011 December 20). This reprocessing eliminated Earth occultations, South Atlantic Anomaly passages and other high-background periods. Light curves and spectra from all three detectors were then extracted using XSELECT, with circular source regions ∼200 arcsec in radius centred on the nucleus. Background regions were made as large as possible while avoiding contamination from both the AGN and the calibration sources in the corners of each detector.

For the XIS spectra, we combined data from the front-illuminated (FI) detectors XIS 0+3 data using the `addascaspec` script in order to increase S/N. The FI and back-illuminated (BI; XIS 1) XIS spectra, responses and backgrounds were then rebinned to 512 spectral channels from the original 4096 using `rbnpha` and `rbnrmf` in order to speed up spectral model fitting without compromising the resolution of the detectors. Finally, the XIS spectra were grouped into a minimum of 25 counts per bin using `grppha` in order to facilitate robust χ^2 fitting. The merged, background-subtracted, time-averaged FI spectrum of 2010a (2010b) has a net 0.7–12 keV count rate of 0.180 ± 0.001 (0.134 ± 0.001) counts s^{-1} for a total of 59 913 (92 736) counts. The total number of 2–10 keV counts is 40 871 (55 285). The total BI count rate is 0.186 ± 0.001 (0.148 ± 0.001)counts s^{-1} for a total of 37 226 (62 326), or 20 038 (28 783) counts when restricting to 2–10 keV. See Table 1 for details. For all of the fitting presented in this paper we allow for a global flux cross-normalization error between the FI and BI spectra. The BI/FI cross-normalization is fixed at 1.03, in accordance with its expected value.[4]

For the Hard X-ray Detector (Takahashi 2007), the PIN instrument detected NGC 1365 in both observations, though the GSO did not. Data from PIN were first reprocessed using the `aepipeline` script, and were then reduced as per the *Suzaku* ABC Guide. For background subtraction, we used the 'tuned' non-X-ray background (NXB) event files for 2010 June and July from the *Suzaku* CALDB,

[3] http://heasarc.gsfc.nasa.gov/docs/suzaku/analysis/abc/

[4] *Suzaku* Memo 2008-06: http://heasarc.gsfc.nasa.gov/docs/suzaku/analysis/watchout.html

Table 1. Observation data for the three *Suzaku* data sets of NGC 1365 discussed in this work. Count rates and total counts are over the 0.7−12 keV energy band for the XIS instrument, and represent the co-added XIS-FI data only. Count rates and total counts are taken over the 14−40 keV band for the PIN instrument.

Date	Time (ks)	XIS (counts s^{-1})	XIS (counts)	PIN (counts s^{-1})	PIN (counts)
2008 January 21	160	0.33	52 800	0.10	16 000
2010 June 27	150	0.18	59 913	0.08	12 000
2010 July 15	300	0.13	92 736	0.07	21 000

along with the appropriate response files and flat-field files for epoch nine data. The NXB background in 2010a (2010b) contributed a count rate of 0.479 ± 0.001 (0.497 ± 0.001)counts s^{-1} to the total X-ray background from 14 to 40 keV, our energy range for adequate S/N. We modelled the cosmic X-ray background (CXB) contribution as per the ABC Guide, simulating its spectrum in XSPEC (Arnaud 1996). The simulated CXB spectrum contributed a count rate of 0.0223 ± 0.0001 (0.0221 ± 0.0001)counts s^{-1} to the total X-ray background from 14 to 40 keV. The NXB and CXB files were combined to form a single PIN background spectrum. In comparison, the PIN data had a count rate of 0.540 ± 0.002 (0.564 ± 0.002)counts s^{-1} over the same energy range.

Because the PIN data only contain 256 spectral channels (versus the 4096 channels in the unbinned XIS data), rebinning to 25 counts per bin was not necessary in order to facilitate χ^2 fitting. Rather, we rebinned the PIN spectrum to have an S/N of 5 in each energy bin, which limited our energy range to 14−40 keV. After reduction, filtering and background subtraction, the PIN spectrum of 2010a (2010b) had a net 14−40 keV count rate of 0.084 ± 0.003 (0.066 ± 0.003)counts s^{-1}, equating to a total of 12 000 (21 000) counts over this energy range (see Table 1). We also added 3 per cent systematic errors to the PIN data to account for the uncertainty in the NXB data supplied by the *Suzaku* calibration team. For the spectral fitting presented in this paper, we assume a PIN/XIS-FI cross-normalization factor of 1.16 as per the *Suzaku* memo 2008-06.[5]

3 TIMING ANALYSIS

The light curves and hardness ratios for the three *Suzaku* observations of NGC 1365 are shown in Fig. 1. The count rate of the 2008 data varies by a factor of ∼3, whereas the count rate of the 2010a data varies by a factor of ∼1.8 and the count rate of the 2010b data, which has the lowest overall flux of the three data sets, varies by only a factor of ∼1.3. This pattern demonstrates, at least to first order, the expected correlation between source flux and variability (Uttley & McHardy 2001) in actively accreting black hole systems.

It is evident that NGC 1365 is much brighter and softer in 2008 than in 2010. Note also the clear anti-correlation between source flux and hardness ratio in 2008 compared with the relatively flat hardness ratios in 2010a and 2010b. The presence of a cold absorbing structure in the nucleus of NGC 1365 is well established (Risaliti et al. 2005b, 2007, 2009a,b,c; Maiolino et al. 2010), with variations in the cold column density by factors of up to ∼10 having been reported between and within previous observations with *Chandra, XMM* and *Suzaku*. The observed trend in source flux and hardness ratio here is consistent with this physical scenario. In the framework of this interpretation, we can infer that the source is relatively unobscured in 2008, but shows distinct eclipses signified by spikes in the hardness ratio coincident with dips in the X-ray light curve. By contrast, the source is both harder and dimmer overall in 2010, decreasing in flux and increasing in hardness in the two weeks between 2010a and 2010b, signifying an increasing column density of the absorber. Additionally, we note two other (though more subtle than 2008) possible eclipse events in each 2010 observation: intervals #2 and #5 in 2010a and #2 and #6 in 2010b. Though these intervals mark times of lower source flux, the hardness ratio during these intervals does not vary as significantly as in the 2008 eclipses, implying either that the change in column density during each 2010 event is not as great as that of the eclipses on 2008 or that the column density itself is high enough that its variation does not significantly impact the hardness ratio (see Fig. 2).

The variation of the source flux versus energy for the XIS data from each observation is shown in Fig. 2. In each case, the root-mean-square fractional variability (RMS $F_{\rm var}$) increases with energy. A high-energy component that varies more than the component best describing the low-energy emission strongly suggests the presence of inner disc reflection signatures in the spectrum. The prominent dip in RMS $F_{\rm var}$ that occurs between 6 and 7 keV at approximately the location of the Fe K complex also indicates the presence of a narrow Fe Kα line fluoresced from distant material (e.g. the outer disc or putative torus of Seyfert unification schemes), which would vary much less, and on time-scales much longer than inner disc reflection signatures seen in and around the same energy range. Most of the variation between the RMS $F_{\rm var}$ of the 2008 and 2010a observations takes place from 3 to 5 keV, in the region dominated by the effects of the power-law continuum, the cold absorbing column and the broad red wing of the Fe Kα line. The key question is which of these components is the primary driver of the spectral changes noted within and between these observations.

Difference spectra for the three observations of NGC 1365 are shown in Fig. 3, illustrating the variations in spectral shape that result when the co-added low-flux XIS and PIN spectra are subtracted from the co-added high-flux XIS and PIN spectra. The change in spectral shape above 3 keV for the 2008 observation is well modelled by a change in both the power-law flux and cold absorber column. By contrast, the change in spectral shape for both 2010 observations is accounted for almost entirely by a change in the cold absorber column, with only a minor contribution from a change in the inner disc reflection. This conclusion will be discussed in greater depth with our analysis of the spectral data in Section 4.1.

4 SPECTRAL ANALYSIS

We begin our spectral analysis by examining the time-averaged spectra of 2010a and 2010b in conjunction with that of the 2008 data in order to examine the changes in spectral shape and flux that the source exhibits over both weeks- and years-long time-scales.

The physical merit of analysing the time-averaged spectra is questionable because of the eclipses by clouds of varying densities during the observations and the changes in spectral shape

[5] http://heasarc.gsfc.nasa.gov/docs/suzaku/analysis/watchout.html

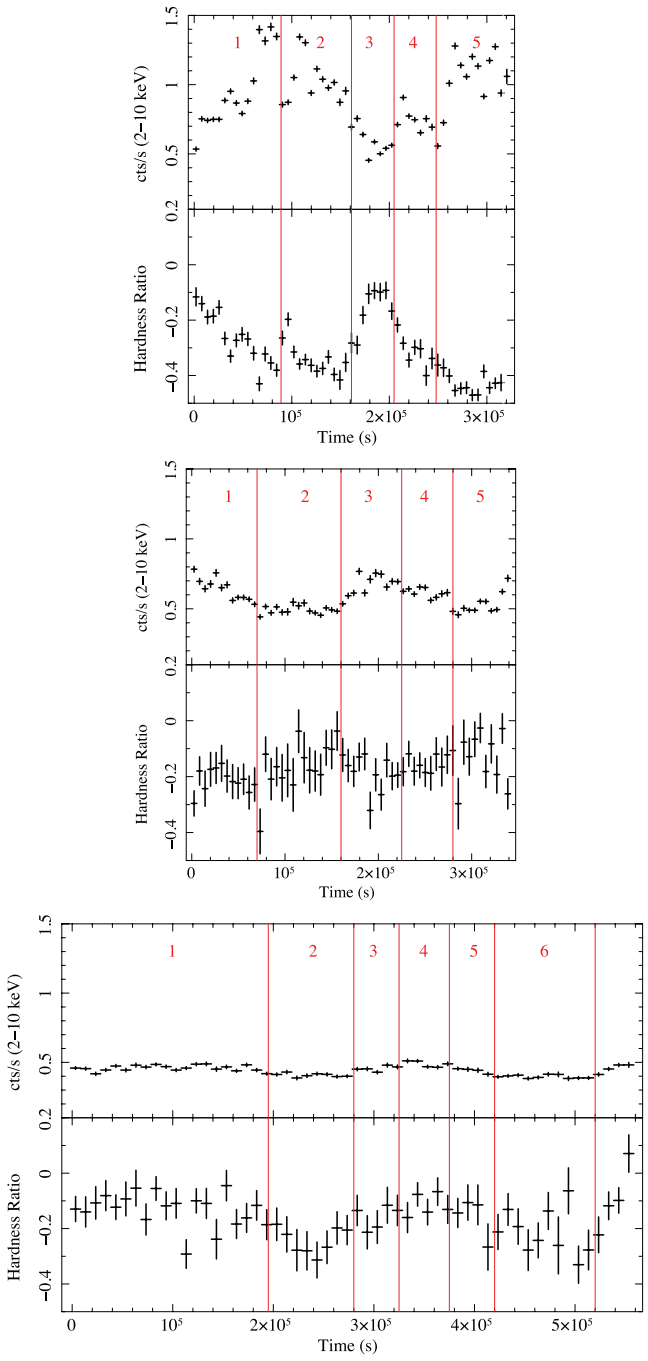

Figure 1. Light curves and hardness ratios for the three *Suzaku* observations of NGC 1365. Time bins are 5.9 ks for 2008 and 2010a and 11.8 ks for 2010b due to its longer exposure time. Hardness ratio is defined as (hard−soft)/(hard+soft) flux, where the hard band extends from 6 to 10 keV and the soft band covers 2–5 keV. Top: the 2008 observation is divided into five time intervals based primarily on source flux; these intervals are shown by the red vertical lines and numbers. Note the anticorrelation between source flux and hardness ratio, a strong indicator of eclipse events. Middle: 2010a also has five time intervals; intervals #2 and #5 are periods of lowest flux. Overall the source is less variable in flux than in 2008, and the hardness ratio is correspondingly less variable. Bottom: 2010b is divided into six time intervals based on flux, with periods of lowest flux in intervals #2 and #6. The observation is roughly twice the length of 2008 and 2010a. 2010b has the lowest source flux of the three observations and also the least amount of variability in both flux and hardness ratio.

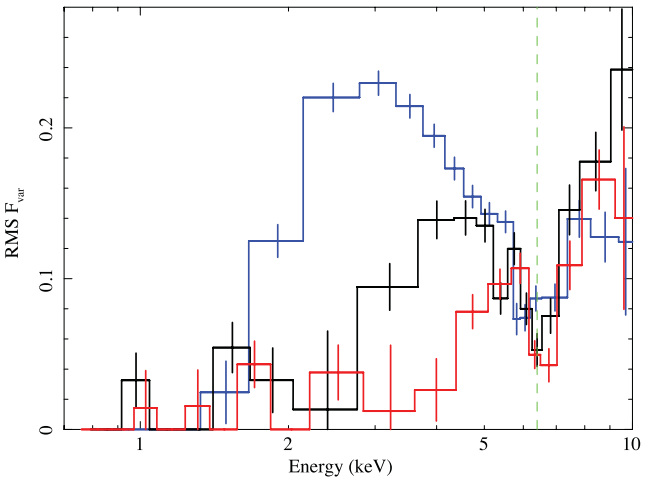

Figure 2. RMS F_{var} spectra for the combined XIS data from 2008 (blue, highest), 2010a (black, middle) and 2010b (red, lowest). Note the lack of variability at energies below ∼2 keV, where the distant starburst emission dominates. The increase in variability is noteworthy at energies above this point, which are dominated by a combination of the continuum, reflection and intrinsic absorption; the 2008 data are especially variable in this region. The dip in variability at ∼6.4 keV (marked by the dashed green line) seen in all three observations suggests that the Fe Kα line has a substantial contribution from distant material that is slow to respond to continuum variations. The overall increase in variability above ∼5 keV in all observations likely represents variable reflection from the inner accretion disc. The intrinsic absorber dominates the 3–5 keV range, showing a steadily decreasing variability from 2008 through 2010a and 2010b.

resulting from these occultations. However, the high S/N, time-averaged spectra can be used to identify the various physical components that must be included in order to model the data accurately. We interpret the parameter values returned by these fits as fiducial in nature, providing a starting point within the parameter space for our subsequent time-resolved spectral analysis, which provides a more accurate representation of the variation of the physical parameters describing the nucleus of NGC 1365.

We explored the parameter space of each model we employed using the Markov chain Monte Carlo (MCMC) algorithm within XSPEC. This procedure is especially effective for thoroughly probing complex, multidimensional parameter spaces (e.g. Reynolds et al. 2012). To assess the parameter space of a given model, four independent, 55 000-element chains were created, each beginning at a different random seed within the parameter space. The first 5000 elements of each chain were discarded during a 'burn-in' phase. A diagonal, Gaussian proposal was used to create the chains, beginning with the squares of the 1σ XSPEC-derived errors on the initial fit of the model to the data. The covariance matrix was then rescaled iteratively until a parameter variance within the chain of ∼0.75 was achieved for each run. The Rubin–Gelman convergence criterion of ∼1 was achieved for each chain. All errors quoted for our resulting spectral fits are derived from the combined 200 000-element chain and correspond to 90 per cent probability, unless otherwise specified.

4.1 Time-averaged spectra

An examination of the time-averaged spectra extracted from each of the three *Suzaku* observations of NGC 1365 presents several features which are readily apparent, over and above the standard power-law continuum describing all AGN: a constant soft

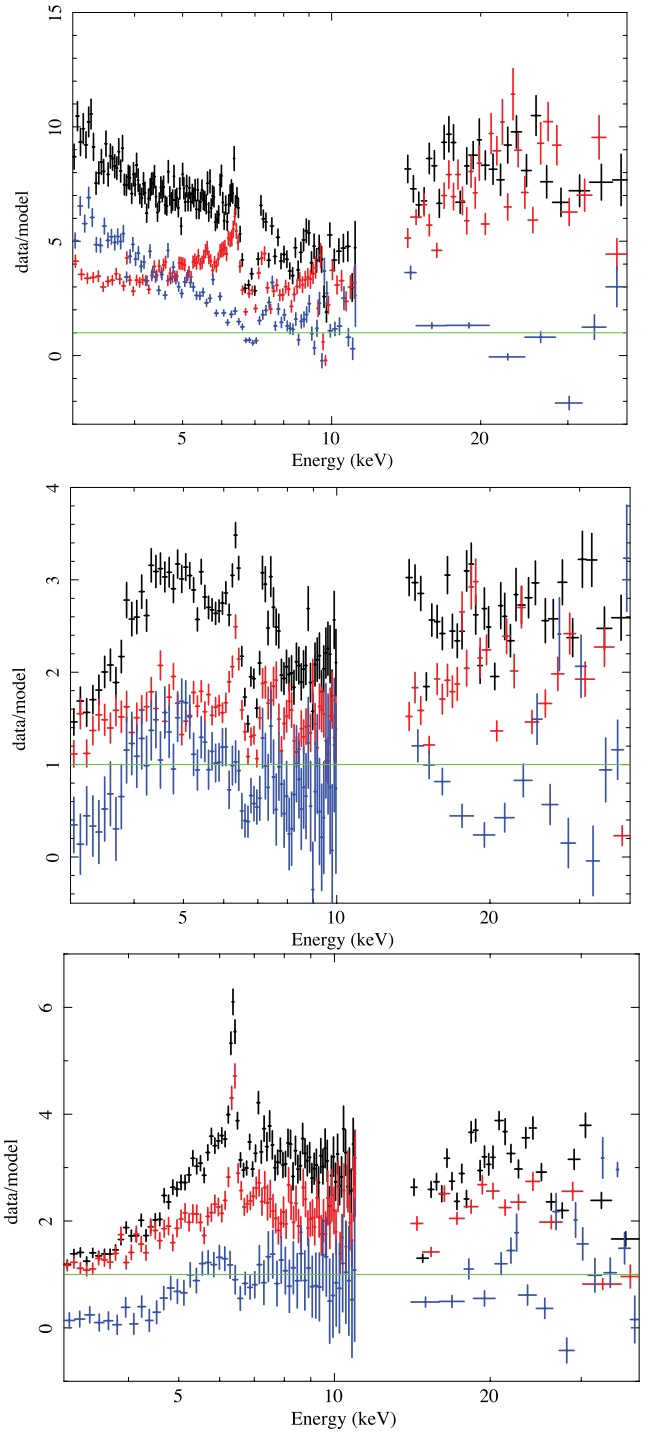

Figure 3. Top: high-flux (black, highest) versus low-flux (red, middle) spectra from the five time intervals in the 2008 data, plotted along with the difference spectrum (high–low; blue, lowest). The spectra are ratioed against an absorbed power law, with the parameters fixed at their time-averaged values except for the power-law normalization, which is allowed to vary freely. The green line represents a data-to-model ratio of unity. Middle: the same plot, now representing the 2010a data. Bottom: the same plot, now for the 2010b data. The change in spectral shape for the 2008 observation is well modelled by a change in the power-law flux and cold absorber column. By contrast, the change in spectral shape for both 2010 observations is best accounted for not only by a change in the cold absorber column and power-law flux, but also by a modest change in the inner disc reflection.

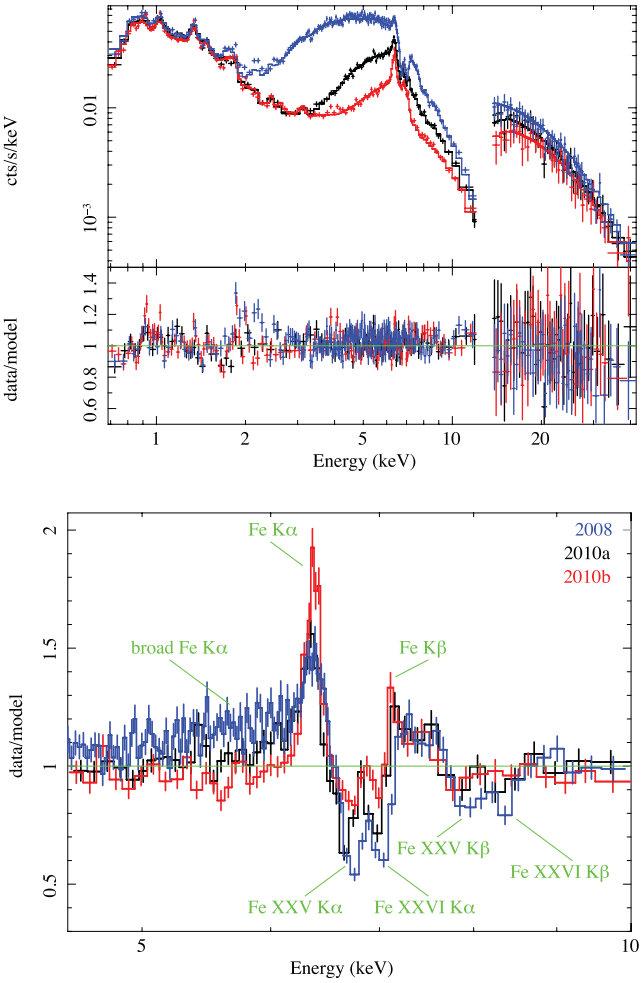

Figure 4. Top: time-averaged spectra for the data from 2008 (XIS-FI and PIN in blue, highest), 2010a (XIS-FI and PIN in black, middle) and 2010b (XIS-FI and PIN in red, lowest). The data/model ratio with respect to our best-fitting model (Table 2) is shown in the lower panel (the green line indicates a theoretical perfect fit). These residuals are dominated by calibration features in the 1.5−2.5 keV range, especially, which we ignore in our model fitting but show here for completeness. Bottom: data-to-model ratio plot for the Fe K region, this time with the warm absorber, broad Fe Kα and narrow Fe emission lines removed from the best-fitting model in order to show the residuals of these features. Colour scheme is the same as for the top panel, with emission and absorption lines labelled in green. The lines connecting data points are meant to guide the eye and do not represent a model. Note the more prominent broad Fe Kα line in 2008 and the more prominent narrow Fe Kα line in 2010b.

component below 2 keV due to a circumnuclear starburst component [resolved by *Chandra* and detailed in Wang et al. (2009), but not focused on here in favour of examining the properties of the nucleus], a highly changeable region from ∼2 to 5 keV in which the curvature is due to a variable cold absorbing column of gas, narrow Fe K emission line(s) from 6 to 7 keV with a subtle curvature on the red wing suggesting the presence of a broad Fe Kα line, variable narrow Fe K absorption lines in the 6–7 keV range indicative of ionized gas within the system, and slightly variable curvature above 10 keV due to reflection of the primary continuum from the disc and/or distant torus. These features can be seen in the spectra and models shown in Figs 4 and 5, and the best-fitting model and parameter values describing each observation are shown in Table 2.

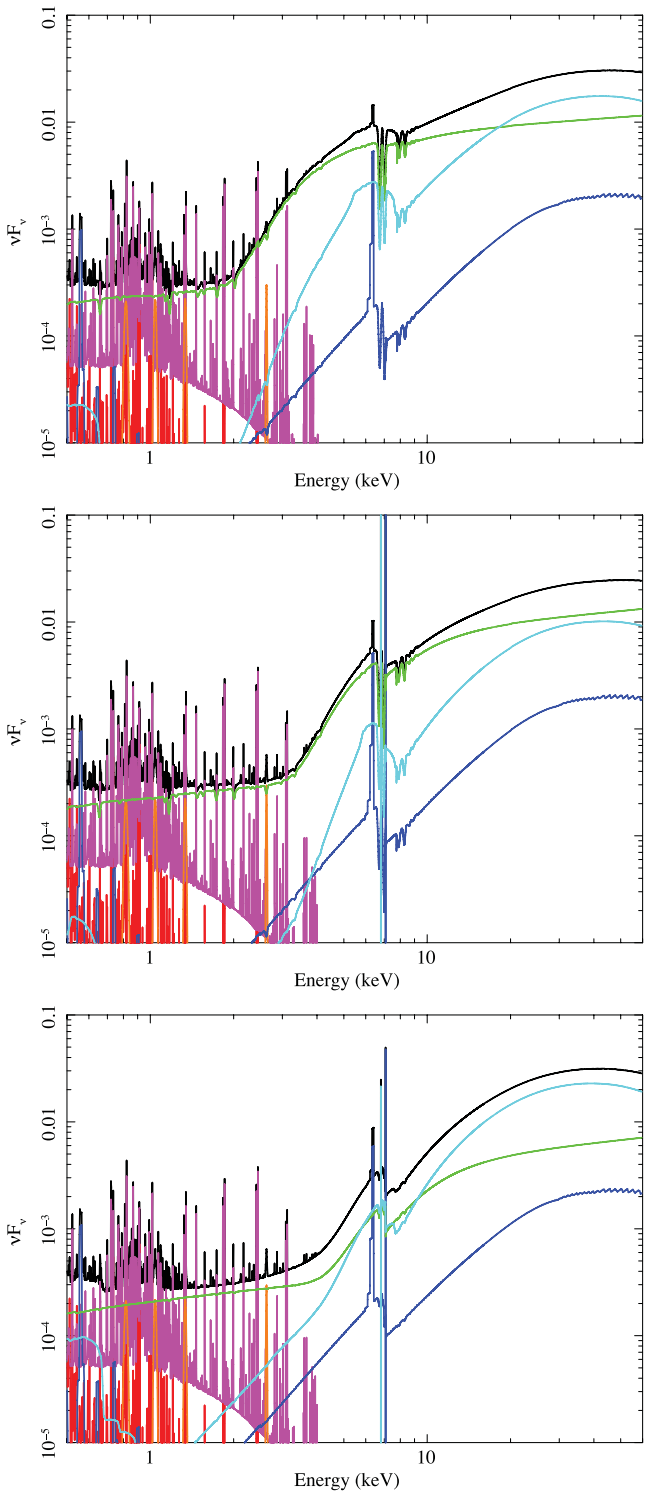

Figure 5. Top: νF_ν plot of the best-fitting model components for the 2008 data. The absorbed power law making up most of the model flux is in green, the two-temperature thermal starburst plasma is shown below ∼3 keV in red and magenta, distant reflection is in dark blue and inner disc reflection is in light blue. The total spectral model is in black. Middle: same as the left-hand panel, but for the 2010a data. Bottom: same as the left-hand panel, but for the 2010b data. Note that the starburst emission is constant between observations, with variability only seen in the spectrum above 3 keV.

Operationally, we model these physical components with the following functional form: `TBabs*(2vapec+4zgauss+ WA*(reflionx+ zpcfabs*(powerlaw+zgauss+relconv (reflionx))))`. This type of model and its components are commonly used to describe AGN spectra showing similar reflection and absorption features to NGC 1365, e.g. MCG-6-30-15 (Fabian et al. 2002; Brenneman & Reynolds 2006; Chiang & Fabian 2011) and NGC 3783 (Brenneman et al. 2011; Patrick et al. 2011; Reynolds et al. 2012). The parameter values and 90 per cent confidence errors for each model component are presented in Table 2, which represents a joint fit to all three time-averaged spectra. The two-temperature thermal plasma ($kT_1 = 0.3$ keV, $kT_2 = 0.69$ keV) and four Gaussian lines ($E_1 = 0.82$ keV, $EW_1 = 10$ eV, $E_2 = 1.05$ keV, $EW_2 = 12$ eV, $E_3 = 1.34$ keV, $EW_3 = 16$ eV, $E_4 = 2.64$ keV, $EW_4 = 24$ eV) representing the starburst emission are held constant at the parameter values determined by Wang et al. (2009).

The warm absorber (WA) in NGC 1365 manifests primarily in the Fe K band as a series of four prominent absorption lines (the Kα and Kβ lines of Fe XXV and Fe XXVI) which have been discussed extensively in Risaliti et al. (2005a, 2007). We model this component with an XSTAR (v2.2.0)[6] multiplicative table within XSPEC, generated specifically for NGC 1365 and identical to the one used in Walton et al. (2010). The free parameters are the column density and ionization parameter of the gas, its redshift (a proxy for outflow velocity) and its iron abundance (which we tie to the iron abundance of the reflection components). This WA has a relatively high ionization of $\xi \geq 3000$ erg cm s^{-1} in all three observations, though its column density increases by a factor of ∼2 between 2008 and 2010a, and then decreases by a factor of ∼10 in the two weeks between 2010a and 2010b. This variability appears to be unrelated to the variability of other components in our time-averaged spectral fitting. Additionally, the absorption lines which comprise the WA are all blueshifted, as noted by Risaliti et al. (2005a, 2007). The outflow velocity of the gas also varies between observations, going from $v_{\rm out} = 3651^{+231}_{-360}$ in 2008 to $v_{\rm out} = 1884^{+285}_{-600}$ in 2010a to $v_{\rm out} = 2961^{+560}_{-1380}$ km s^{-1} in 2010b. Though the 2010 observations do not demonstrate significant variability in two weeks, taking errors into account, the change in the outflow velocity does appear to be robust at the ∼4σ level on 2 yr time-scales.

The distant reflector is modelled by a `reflionx` component (Ross & Fabian 2005) with its ionization fixed at ∼neutral ($\xi = 1$ erg cm s^{-1}), its incident power-law index tied to that of the power-law component (PLC) and its iron abundance tied to that of the WA. The normalization of this component does not vary significantly between the three observations. In addition to the narrow Fe Kα and Kβ emission lines that are the most prominent features of this distant reflection, we also note a possible narrow line of ionized iron at 6.84 keV in both of the spectra from 2010, though this feature is only statistically significant in 2010a. The line is unresolved and its width is therefore fixed at 10 eV, but, if present, it would suggest that the distant reflector is not entirely composed of neutral gas. Allowing the ionization parameter of the distant `reflionx` component to vary yields only an upper limit of $\xi \leq 1.2$, however, so we have elected to continue with ξ fixed at unity.

We note that the cold absorbing column (`zpcfabs`) is quite prominent in NGC 1365, averaging a density of $(1.5^{+0.3}_{-0.2}) \times 10^{23}$ cm^{-2} in

[6] The latest release of the XSTAR software (v2.2.1) has several updates to the atomic data for iron, which result in larger measured column densities when using v2.2.1. Using an identical table model generated with v2.2.1, we note that the column densities derived from the data increase by a factor of ∼2.

Table 2. Best-fitting parameters and their errors (to 90 per cent confidence for one interesting parameter) for the joint spectral modelling of the time-averaged data sets for the 2008, 2010a and 2010b observations. Only the XIS-FI and PIN data are included. The energy range covered is 0.7–1.5 and 2.5–40.0 keV, though only model components relevant for $E \geq 3$ keV are listed here since the spectrum below this energy is dominated by extended, non-nuclear emission (Wang et al. 2009). Galactic column is fixed at $N_{\rm H} = 1.34 \times 10^{20}\,{\rm cm}^{-2}$, as per Kalberla et al. (2005). The power-law indices of the `reflionx` components were tied to that of the primary PLC, and the iron abundance of the WA was tied to that of the two `reflionx` components for consistency. Unless otherwise specified, redshifts were fixed at the cosmological value for NGC 1365: $z = 0.005\,47$. The values marked with an asterisk (*) were tied between epochs while those marked with an (*f*) were fixed during the fit.

Component	Parameter (units)	2008	2010a	2010b
TBabs	$N_{\rm H}$ (cm^{-2})	$1.34 \times 10^{20}(f)$	$1.34 \times 10^{20*}$	$1.34 \times 10^{20*}$
WA	$N_{\rm H}$ ($\times 10^{22}$ cm^{-2})	$5.95^{+0.37}_{-0.34}$	$10.33^{+0.72}_{-1.32}$	≤ 1.48
	ξ (erg cm s^{-1})	3019^{+369}_{-135}	5495^{+814}_{-483}	3019^{+696}_{-389}
	$v_{\rm out}$ (km s^{-1})	3651^{+231}_{-360}	1884^{+285}_{-600}	2961^{+570}_{-1380}
Reflionx (distant)	Fe/solar	$3.5^{+0.3}_{-0.1}$	3.5*	3.5*
	$K_{\rm Rdist}$ (ph cm^{-2} s^{-1})	$3.9^{+0.3}_{-0.7} \times 10^{-5}$	$3.8^{+0.4}_{-1.0} \times 10^{-5}$	$4.3^{+0.1}_{-0.2} \times 10^{-5}$
Zpcfabs	$N_{\rm H}$ ($\times 10^{22}$ cm^{-2})	$15.4^{+0.3}_{-0.2}$	$58.3^{+0.5}_{-0.6}$	$106.6^{+5.3}_{-3.2}$
	$f_{\rm cov}$	$0.95^{+0.01}_{-0.01}$	$0.95^{+0.01}_{-0.01}$	$0.91^{+0.01}_{-0.01}$
Power law	Γ	$1.81^{+0.04}_{-0.04}$	$1.76^{+0.02}_{-0.03}$	$1.73^{+0.01}_{-0.13}$
	$K_{\rm PL}$ (ph cm^{-2} s^{-1})	$5.43^{+0.37}_{-0.27} \times 10^{-3}$	$4.92^{+0.20}_{-0.18} \times 10^{-3}$	$2.30^{+0.41}_{-0.02} \times 10^{-3}$
Zgauss	E (keV)	$6.84^{+0.13}_{-0.14}$	6.84*	6.84*
	σ (keV)	0.01(*f*)	0.01*	0.01*
	$K_{\rm line}$ (ph cm^{-2} s^{-1})	$0.0^{+0.7}_{-0.0} \times 10^{-5}$	$2.3^{+0.7}_{-0.3} \times 10^{-5}$	$0.5^{+0.2}_{-0.1} \times 10^{-5}$
	EW (eV)	0^{+1}_{-0}	93^{+28}_{-12}	28^{+11}_{-6}
Relconv	q	$5.9^{+0.2}_{-0.3}$	$6.9^{+2.1}_{-1.0}$	$5.4^{+0.3}_{-0.4}$
	$r_{\rm in}$ ($r_{\rm g}$)	$1.9^{+0.1}_{-0.1}$	$2.0^{+0.1}_{-0.1}$	$1.3^{+0.2}_{-0.1}$
Reflionx (inner)	ξ (erg cm s^{-1})	≤ 2.0	≤ 2.0	$1.7^{+1.2}_{-0.4}$
	$K_{\rm Rrel}$ (ph cm^{-2} s^{-1})	$4.06^{+0.05}_{-2.10} \times 10^{-4}$	$2.34^{+0.04}_{-1.30} \times 10^{-4}$	$3.50^{+0.10}_{-1.80} \times 10^{-4}$
F_{2-10}	Absorbed (erg cm^{-2} s^{-1})	1.27×10^{-11}	6.13×10^{-12}	4.05×10^{-12}
L_{2-10}	Absorbed (erg s^{-1})	8.37×10^{41}	4.02×10^{41}	2.65×10^{41}
F_{2-10}	Unabsorbed (erg cm^{-2} s^{-1})	2.25×10^{-11}	2.12×10^{-11}	1.59×10^{-11}
L_{2-10}	Unabsorbed (erg s^{-1})	1.49×10^{42}	1.40×10^{42}	1.05×10^{42}
Joint fit	χ^2/ν	3063/2668 (1.15)		

2008 and increasing steadily to $(5.8^{+0.5}_{-0.6}) \times 10^{23}\,{\rm cm}^{-2}$ 2 years later in 2010a and $(10.7^{+0.5}_{-0.5}) \times 10^{23}\,{\rm cm}^{-2}$ two weeks later in 2010b. It has a covering factor (denoted by $f_{\rm cov}$) over the hard X-ray source and inner disc, which is (95 ± 1) per cent in 2008 and 2010a, but decreases to (91 ± 1) per cent in 2010b at the 4σ level. Given its high value, we interpret this covering factor physically as a scattered fraction, rather than as a formal partial-covering absorber.

The photon indices of the PLCs do not vary significantly ($\leq 2\sigma$) between observations ($\Gamma \sim 1.75$), and the normalization of the power law is constant within 10 per cent from 2008 to 2010a, but drops by a factor of $\sim$2 ($\geq 6\sigma$) in the two weeks between 2010a and 2010b.

The inclusion of an inner disc reflection component, parametrized above by `relconv(reflionx)`, is necessary in order to achieve a statistically adequate model fit to the data in each of our three time-averaged observations, in spite of the variation in spectral state between them. Eliminating this component and refitting the time-averaged data worsens the global goodness of fit by $\Delta\chi^2/\Delta\nu = +385/+14$ and clearly results in a poor fit to the eye with large residuals in the 3–10 keV region (see Fig. 6).

As with the distant reflector, we have tied the iron abundance of the inner disc reflector to that of the WA, and the index of the incident power-law radiation to that of the PLC. The ionization of the inner disc reflector does not appear to deviate significantly from neutrality in any of the observations. We further note that the normalization of this component is nearly 10 times that of the distant reflector, but it does not vary significantly, dropping by a factor of $\sim$1.8 from 2008 to 2010a (at only 0.8σ) and by an additional factor of $\sim$1.2 between 2010a and 2010b (at only 0.9σ).

We convolve the inner disc reflector with a `relconv` smearing kernel (Dauser et al. 2010), which imprints the effects of relativistic Doppler shifts from the rotating disc and general relativity from the central supermassive black hole on to the spectrum. We assume that the disc is inclined at $i = 58^\circ$, in keeping with the results of Risaliti et al. (2005b, 2007, 2009a), Maiolino et al. (2010) and Walton et al. (2010). We also assume that the disc radiates $\propto r^{-q}$, where q is allowed to vary freely and the emitting portion of the disc extends from $r_{\rm in}$ to $r_{\rm out} = 400\,r_{\rm g}$ for a maximally spinning black hole, where $r_{\rm in}$ is also allowed to vary freely. This approach allows us to directly compare our results to a previous work: $q = 5.0^{+1.0}_{-0.5}$ in the 2008 *Suzaku* observation analysed by Walton et al. (2010), and it is measured between $q = 5$ and 9 – constant within errors – in the three *Suzaku* observations considered here (our measured $q = 5.9^{+0.2}_{-0.3}$ in 2008 is entirely consistent with Walton et al., within errors). Our

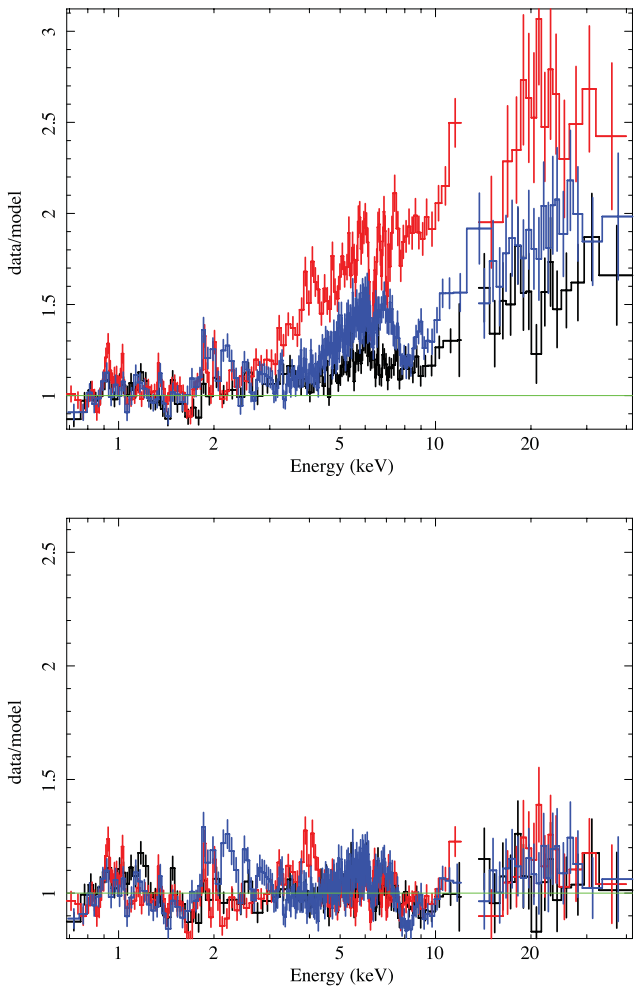

Figure 6. Top: the ratio for the best-fitting model to the data from the three *Suzaku* observations of NGC 1365, with the inner disc reflection component subtracted in order to illustrate the spectral features fitted by this component. 2008 data are shown in blue (middle), 2010a in black (lowest) and 2010b in red (highest). Bottom: same as the top plot, but this time the best-fitting model without inner disc reflection has been refitted, yielding a significantly worse fit by $\Delta\chi^2/\Delta\nu = +385/+14$ compared with the best-fitting model. This demonstrates the importance of this component to the global goodness of fit.

measured inner disc radius, assumed to be the ISCO, is constant within errors between 2008 and 2010a ($r_{\rm in} = 1.9^{+0.1}_{-0.1}{-}2.0^{+0.1}_{-0.1}\,r_{\rm g}$), but drops to $r_{\rm in} = 1.3^{+0.2}_{-0.1}\,r_{\rm g}$ in 2010b. This change is only significant at the 1.8σ level, however. We note that our 2008 measurement is consistent with that of Walton et al. as well ($r_{\rm in} = 1.85 \pm 0.15\,r_{\rm g}$).

The low inner disc radii measured from the data suggest a rapidly rotating, prograde black hole with a spin of $a \geq 0.93$, provided that the inner edge of the disc measured here is indeed the ISCO. If instead we fix the inner radius of the disc to $r_{\rm in} = r_{\rm ISCO}$ for each observation and allow the black hole spin to vary freely (linking the spin value between observations), we measure $a = 0.96 \pm 0.01$ (where $a \equiv cJ/GM^2$ for a supermassive black hole of mass M and angular momentum J). Because the measurement of black hole spin in NGC 1365 is not the focus of this paper, however, we do not perform a rigorous analysis of the spin determination and sources of error here. This analysis will be presented in a forthcoming paper (Brenneman et al., in preparation).

An examination of the unabsorbed fluxes and luminosities of NGC 1365 in Table 2 indicates that the source was brightest in 2008 and dimmest in 2010b, though the difference in unabsorbed power (factor of 1.4 between the three observations) is less than that of the absorbed power (factor of 2.0 between the observations), indicating that absorption plays a significant role in shaping the spectrum of the AGN. Indeed, the change of the power-law normalization and inner disc reflection components alone cannot account for the change in spectral shape in the range $\sim$2−5 keV between 2008, 2010a and 2010b. Attempting to account for the change entirely with the power law and inner disc reflector results in a worsening of the fit by $\Delta\chi^2/\Delta\nu = +3237/+2$ and a clearly inadequate visual match to the data. This reinforces the hypothesis that the primary driver of the spectral shape change between the three observations is the cold absorbing column.

Previous studies (e.g. Risaliti et al. 2009a) have cited the need for a second cold absorber to explain the hard energy excess $\geq$10 keV. We note that, as per Walton et al. (2010), the requirement for such a component ($f_{\rm cov} = 100$ per cent) disappears if we allow the iron abundance of the accretion disc to vary freely in our model fitting: Fe/solar $= 3.5^{+0.3}_{-0.1}$. This value is driven jointly by the presence of the Fe XXV and Fe XXVI Kα and Kβ absorption lines, the strength and shape of the distant reflection features and the strength and shape of the inner disc reflection features (i.e. the Fe Kα line and Compton hump).

4.2 Time-resolved spectra

The lengths and S/N of our three *Suzaku* pointings of NGC 1365 also enabled us to examine the spectral changes of this AGN within each observation. We divided each data set into five (2008, 2010a) or six (2010b) time intervals, which are shown in Fig. 1. These intervals were selected based primarily on the flux changes within each observation, though prominent hardness ratio changes also played a role in helping us identify time intervals in the 2008 observation. Our selected time intervals are designed to focus on changes in the spectral shape of the source from one observation segment to another. The spectra extracted from each time interval in each observation are shown in Fig. 7. We focus on the XIS-FI spectra above 3 keV in order to avoid the energies dominated by the approximately constant circumnuclear starburst emission below $\sim$3 keV. The low energies are still included in the fit, but the starburst parameter values are fixed to those from Wang et al. (2009). The time-averaged PIN spectra for each observation are also shown and are considered in our analysis with a statistical weighting for each time interval corresponding to the length of the time interval as a fraction of the whole observation length, along with a flux normalization corresponding to the flux of the XIS data in each interval relative to the time-averaged XIS flux.

After fitting the time-averaged spectral model from each observation jointly to its time intervals and then allowing all of the parameters to vary between intervals, we have determined that the only model components which vary significantly (i.e. $\geq 3\sigma$) between intervals are, not surprisingly, the cold absorbing column, the power-law flux and the flux of the inner disc reflector. We therefore proceed with our time-resolved spectral fitting for each observation allowing only these three parameters to vary between time intervals and fixing all other parameters to their time-averaged values for that observation. The results of our time-resolved spectral analysis are presented in Table 3, and are shown in Figs 8 and 9.

The variation of the spectral shape between time intervals during each observation is evident to the eye (Fig. 7). An

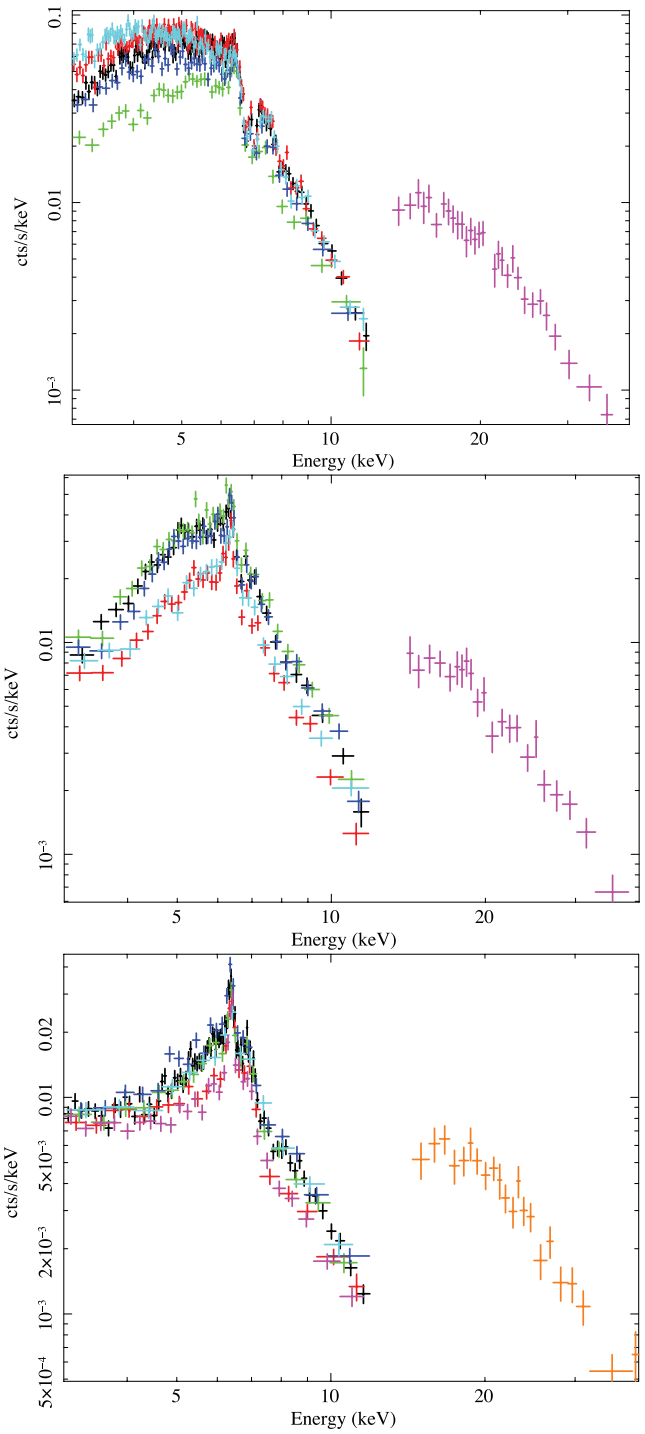

Figure 7. Time-resolved spectra from the five time intervals in 2008 (top panel), 2010a (middle panel) and the six time intervals in 2010b (bottom panel). Spectra shown are XIS-FI only for viewing purposes and extend only from 3 to 10 keV to avoid contamination from the starburst emission below these energies. Time-averaged PIN data are shown for each observation. XIS interval numbers in each panel are colour coded chronologically: black = interval 1, red = 2, green = 3, dark blue = 4, light blue = 5, magenta = 6 (2010b only). PIN data are shown in magenta in 2008 and 2010a and in orange in 2010b.

examination of Table 3 and Figs 8 and 9 suggests that the cold absorbing column and PLC flux are anticorrelated, as are the power-law flux and the flux of the inner disc reflection-dominated component (RDC). Closer inspection of the data and errors in Fig. 9 reveals that this apparent anticorrelation is most significant for the PLC versus $N_{\rm H}$ (12 per cent uncertainty in line slope at 90 per cent confidence due to scatter; Spearman's rank coefficient of $\rho = -0.703$ with the corresponding correlation P-value = 0.001), but is less significant for the PLC versus RDC (27 per cent uncertainty; Spearman's rank coefficient of $\rho = -0.718$ with the corresponding correlation P-value = 0.0008). The RDC versus $N_{\rm H}$ shows a positive correlation with 38 per cent uncertainty (Spearman's rank coefficient of $\rho = 0.871$ with the corresponding correlation P-value = 0.0001).

The 2008 spectra are the brightest of the three epochs and are also the least affected by the cold absorber, having a convex shape below the Fe Kα line (see Fig. 7). The definitive time-resolved spectral analysis of these data has been presented in Maiolino et al. (2010); as such, we do not repeat it unnecessarily, but rather focus our examination on five more coarsely spaced time intervals to illustrate the overall changes in S/N during this observation. Our time-resolved spectra show marked differences from 3 to 6 keV, but above this energy they are nearly identical. Joint spectral fitting of the five time intervals demonstrates that the average column density is $N_{\rm H} = (17.2^{+0.9}_{-1.0}) \times 10^{22}\,{\rm cm}^{-2}$, with a standard deviation of $\sigma = 4.0 \times 10^{22}\,{\rm cm}^{-2}$ between time intervals. The average power-law flux is $\log F_{\rm PLC} = -10.34^{+0.02}_{-0.03}\,{\rm erg\,cm^{-2}\,s^{-1}}$, with $\sigma = 0.13\,{\rm erg\,cm^{-2}\,s^{-1}}$ in log space between intervals, and the average $\log F_{\rm RDC} = -10.58^{+0.04}_{-0.06}\,{\rm erg\,cm^{-2}\,s^{-1}}$ has $\sigma = 0.22\,{\rm erg\,cm^{-2}\,s^{-1}}$ in log space between intervals.

By contrast, the 2010a time-resolved spectra are slightly concave below 6 keV (see Fig. 7), demonstrating that the absorbing column is stronger during this observation than in 2008. The different 2010a time intervals do not show obvious changes in spectral shape, though they do show changes in amplitude, with intervals #2 and #5 clearly having lower flux than intervals #1, #3 and #4 by a factor of $\sim$1.5 (3σ). Joint spectral fitting of the five time intervals in 2010a indicates that the average column density is $N_{\rm H} = (66.7^{+2.6}_{-2.8}) \times 10^{22}\,{\rm cm}^{-2}$, with a standard deviation of $\sigma = 15.9 \times 10^{22}\,{\rm cm}^{-2}$ between intervals. The average power-law flux is $\log F_{\rm PLC} = -10.28^{+0.03}_{-0.03}\,{\rm erg\,cm^{-2}\,s^{-1}}$, with $\sigma = 0.06\,{\rm erg\,cm^{-2}\,s^{-1}}$ in log space between intervals, and the average inner disc reflection flux is $\log F_{\rm RDC} = -10.83^{+0.08}_{-0.16}\,{\rm erg\,cm^{-2}\,s^{-1}}$, with $\sigma = 0.29\,{\rm erg\,cm^{-2}\,s^{-1}}$ in log space between intervals.

The 2010b observation has the lowest flux of the three data sets and is also the most heavily absorbed, as can be seen in its clear concavity below 6 keV (see Fig. 4). Whereas the 2008 and 2010a data showed clear evidence for changes in the cold absorbing column both in their model fits and to the eye, the 2010b data do not show such clear visual changes in absorption. Overall, the spectral shape change is less pronounced than in 2008 and 2010a, and is evenly split between the absorbing column and the power-law flux, with no significant contribution from the inner disc reflector. On average, $N_{\rm H} = (115^{+7}_{-8}) \times 10^{22}\,{\rm cm}^{-2}$, with a standard deviation of $\sigma = 30 \times 10^{22}\,{\rm cm}^{-2}$ between intervals. The $\log F_{\rm PLC} = -10.67^{+0.05}_{-0.10}\,{\rm erg\,cm^{-2}\,s^{-1}}$, with $\sigma = 0.12\,{\rm erg\,cm^{-2}\,s^{-1}}$ in log space between intervals. The $\log F_{\rm RDC} = -10.61^{+0.08}_{-0.09}\,{\rm erg\,cm^{-2}\,s^{-1}}$, with $\sigma = 0.80\,{\rm erg\,cm^{-2}\,s^{-1}}$ in log space between intervals.

We have demonstrated the importance of including relativistic, inner disc reflection in the best-fitting spectral model for the time-averaged data in Section 4.1. This component is equally important in the spectral fitting of the time-resolved data. To illustrate

Table 3. Parameter values and their errors (90 per cent confidence for one interesting parameter) for the best-fitting spectral models for the joint fits of the five time intervals in 2008 and 2010a and the six time intervals of 2010b, respectively. The fit is over the energy range from 3 to 40 keV. Absorbing column is in units of cm^{-2}, and the log values of PLC and inner disc RDC flux are in units of $\mathrm{erg\,cm^{-2}\,s^{-1}}$ as measured over the same energy band.

Observation	Interval	Cold $N_{\rm H}$ ($\times 10^{22}$)	log $F_{\rm PL}$ ($\mathrm{erg\,cm^{-2}\,s^{-1}}$)	log $F_{\rm Rrel}$ ($\mathrm{erg\,cm^{-2}\,s^{-1}}$)
2008	1	$17.5^{+1.3}_{-1.5}$	$-10.31^{+0.04}_{-0.05}$	$-10.40^{+0.06}_{-0.06}$
	2	$14.7^{+1.4}_{-1.0}$	$-10.26^{+0.04}_{-0.03}$	$-10.48^{+0.06}_{-0.09}$
	3	$22.7^{+3.2}_{-4.1}$	$-10.56^{+0.09}_{-0.13}$	$-10.43^{+0.07}_{-0.08}$
	4	$18.8^{+2.4}_{-2.1}$	$-10.34^{+0.06}_{-0.06}$	$-10.66^{+0.13}_{-0.20}$
	5	$12.2^{+0.9}_{-0.8}$	$-10.22^{+0.02}_{-0.02}$	$-10.93^{+0.09}_{-0.14}$
2010a	1	$52.2^{+5.2}_{-5.1}$	$-10.30^{+0.06}_{-0.08}$	$-10.72^{+0.15}_{-0.19}$
	2	$71.4^{+6.2}_{-8.4}$	$-10.36^{+0.06}_{-0.05}$	$-11.22^{+0.23}_{-0.50}$
	3	$55.6^{+6.1}_{-3.7}$	$-10.27^{+0.08}_{-0.06}$	$-10.52^{+0.09}_{-0.16}$
	4	$62.3^{+4.5}_{-4.3}$	$-10.25^{+0.05}_{-0.06}$	$-10.67^{+0.12}_{-0.20}$
	5	$91.9^{+7.0}_{-7.8}$	$-10.21^{+0.05}_{-0.06}$	$-11.04^{+0.28}_{-0.57}$
2010b	1	109^{+8}_{-6}	$-10.69^{+0.04}_{-0.06}$	$-10.25^{+0.06}_{-0.06}$
	2	176^{+22}_{-42}	$-10.89^{+0.24}_{-0.58}$	$-10.08^{+0.13}_{-0.29}$
	3	105^{+15}_{-15}	$-10.65^{+0.06}_{-0.09}$	$-10.38^{+0.14}_{-0.18}$
	4	$95.5^{+12.0}_{-10.2}$	$-10.62^{+0.07}_{-0.09}$	$-10.30^{+0.10}_{-0.10}$
	5	105^{+26}_{-16}	$-10.62^{+0.10}_{-0.15}$	$-10.39^{+0.25}_{-0.26}$
	6	102^{+7}_{-6}	$-10.52^{+0.02}_{-0.03}$	$-12.23^{+0.38}_{-0.34}$
Joint fit	χ^2/ν	4007/3795 (1.06)		

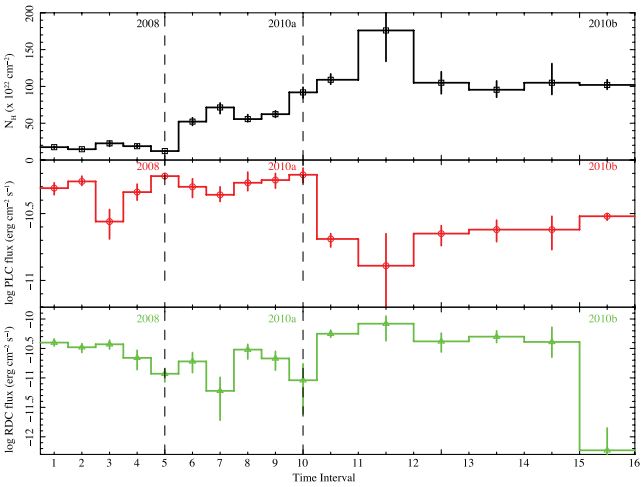

Figure 8. Variations in the cold absorbing column density (top panel), power-law flux (middle panel) and inner disc reflection flux (bottom panel) over the course of the three *Suzaku* observations of NGC 1365. The 2008, 2010a and 2010b data are divided in each panel by the dashed vertical lines. Time intervals are roughly twice as long for 2010b as for 2010a or 2008 since the observation length is roughly doubled.

this, we have shown in Fig. 10 the average residual left behind when the inner disc reflection component (parametrized through `relconv[reflionx]`) is removed from the model in each time interval for each observation. The residuals from each time-resolved interval are then co-added to produce the average residual shown. Note the prominent, asymmetric Fe Kα line and Compton hump that remain unmodelled without the inner disc reflection component.

In order to investigate the nature of the broad iron line and Compton hump separately, we also attempted a model fit replacing the `reflionx` component for the inner disc with a `pexrav` model plus a Gaussian line to represent the Fe Kα emission line core. As with the `reflionx` RDC, we convolved the `pexrav+zgauss` RDC with a `relconv` smearing kernel to account for relativistic effects near the black hole. If the broad line and Compton hump vary in the same sense (i.e. by comparable magnitudes and on comparable time-scales), this would provide additional evidence supporting the relation and physical origin of these two features in a way that `reflionx` (which assumes that they originate from the same material) cannot. Unfortunately, neither the time-resolved spectra nor the time-averaged spectra were able to constrain the parameters of both the `pexrav` and `zgauss` components separately, mainly owing to the high background of the PIN instrument. *NuSTAR* (Harrison et al. 2005) will have both higher collecting area and a lower background than the *Suzaku*/PIN instrument, however. The *NuSTAR* observing campaign on NGC 1365 is already underway and will enable the broad iron line and Compton hump to be constrained separately and simultaneously on these types of short time-scales (Risaliti et al., in preparation).

5 DISCUSSION

5.1 Variability of the cold absorber

Historically, the eclipses of the inner accretion disc and corona (as tracked by the broad Fe Kα line and power-law continuum, respectively) in NGC 1365 have been observed with a broad range of physical parameters. The column density of the occulting gas typically ranges from Compton-thin to Compton-thick, with $N_{\rm H} \sim 2 \times 10^{23}$–$2 \times 10^{24}\,\mathrm{cm}^{-2}$. The covering fraction of the occulting gas ranges from ∼10 to ∼95 per cent between eclipse events, with one notable example of variation from ∼55 to 100 per cent, independent of column density variations, during the

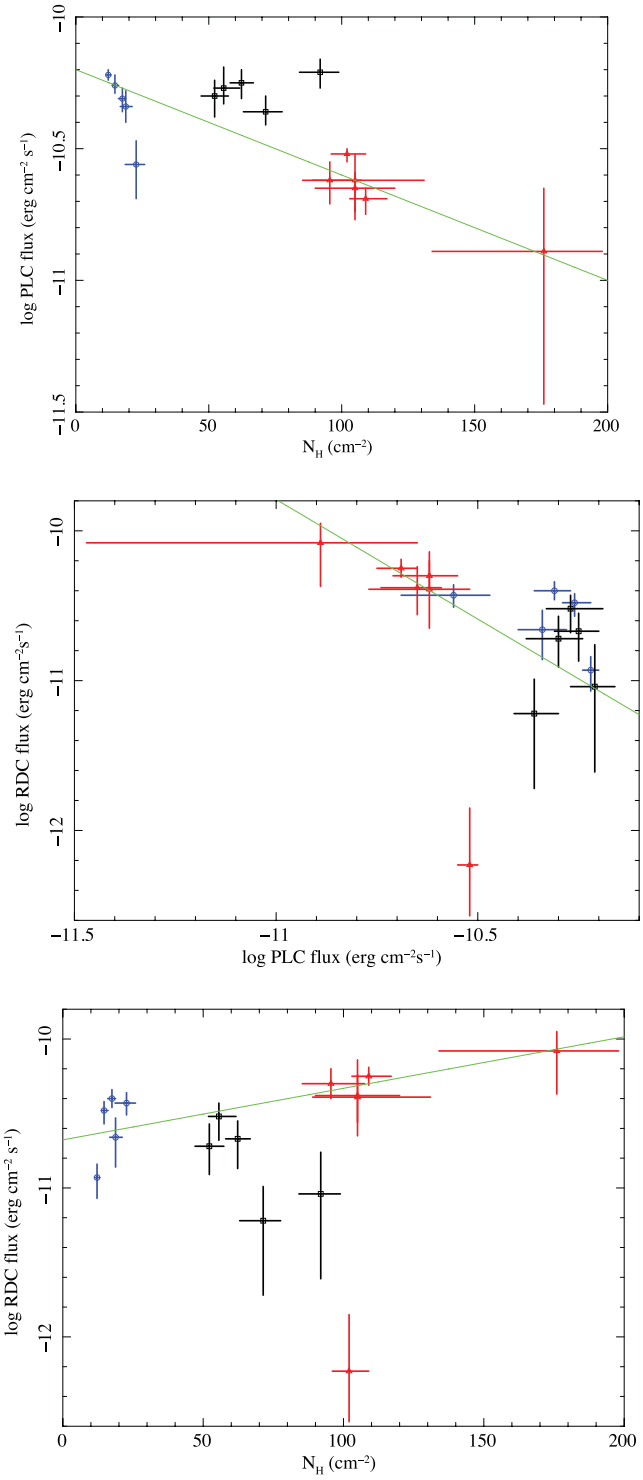

Figure 9. Plot of the variation in the cold absorbing column density (in units of 10^{22} cm^{-2}) versus PLC (top panel), the RDC versus the PLC (middle panel) and the column density versus the RDC (bottom panel) over the course of the three observations. Data points are colour coded: blue circles for 2008, black squares for 2010a and red triangles for 2010b. The solid green line represents a best fit to the data in each panel, neglecting those points with significantly larger errors than the norm. The N_H versus PLC plot does show an apparent inverse correlation, as does the PLC versus RDC plot (though with a higher statistical uncertainty). It then follows that the N_H versus RDC plot shows a corresponding positive correlation, though also with a high statistical uncertainty.

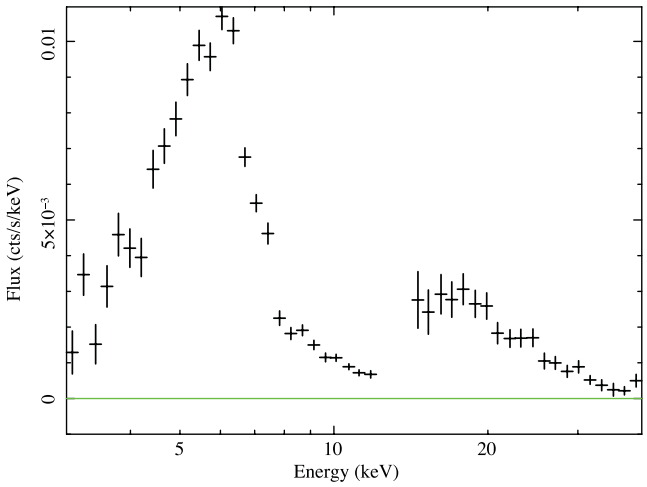

Figure 10. The co-added residual flux of the data above the model, left behind when the inner disc reflector is removed from the fit to all of the time-resolved data sets. This plot depicts the features that the inner disc reflector accounts for in the spectral fit, and the statistical importance of those features.

2008 *Suzaku* observation of the source (Maiolino et al. 2010). Such eclipses have been detected every time NGC 1365 has been observed in X-rays with *Chandra, XMM* or *Suzaku*, and have typical durations of 40–70 ks (Risaliti et al. 2009a; Maiolino et al. 2010). Compton-thin eclipses are seen more commonly than their Compton-thick counterparts, indicating that the gas clumps along the line of sight to the central regions of the AGN most often have $N_H \leq 10^{24}$ cm^{-2} .

Our 2010 observations follow these trends, showing significant variations in flux on time-scales of days and weeks. In both 2010a and 2010b, we note two dips in the X-ray light curves (intervals #2 and #5 in 2010a and #2 and #6 in 2010b; see Fig. 1), though none of the dips is greater than 25 per cent in flux (at 2σ significance), as compared with a $\geq$40 per cent drop in flux (at 10σ significance) seen in the more dramatic 2008 eclipse events. Further, none of the flux decreases seen in 2010 corresponds to a significant change in the hardness ratio as seen in 2008. The 2010a eclipses are all Compton-thin, though all of the 2010b observation borders on a Compton-thick state ($N_H \sim 10^{24}$ cm^{-2}). We also note that the continued increase in the column density of the cold absorber from 2008 through 2010b is a primary contributor to the overall decrease in the flux of NGC 1365 during this time. Interestingly, the variability of the source flux has decreased in accordance with the flux itself, which might imply that the absorbing medium is more uniform in addition to having a greater column density during 2010b than 2010a or 2008 (but see Uttley & McHardy 2001: this direct correlation between source flux and variability is also predicted in systems where the flux is dominated by the coronal PLC, and the corona is flaring, or in scenarios where the mass accretion rate in the disc is fluctuating on short time-scales). Though the density argument is borne out by our spectral fitting, however, the covering fraction of the cold gas in 2010b is actually smaller than in 2010a and 2008 (see Table 2).

The low, relatively constant spectral state witnessed over $\sim$300 ks of on-source observing time in 2010b is a factor of $\geq$4 longer than any previously observed eclipse event, and may imply a new population of larger and/or slower moving cold absorber clouds. One must also acknowledge the role of the diminished power-law flux during this observation as well, however. It is interesting to

note the change in the Fe K emission lines from 2008 to 2010: the narrow line core appears much more prominent during 2010a and peaks in 2010b, while being virtually absent in 2008 (see Fig. 4). The normalization of the distant reflector remains constant during this time. This coincides with the steady increase in the column density of the cold absorber, a diminishing of the broad red wing of the Fe Kα line arising from the inner accretion disc and a diminishing of the flux from the PLC over the same time frame.

In the previous work on NGC 1365 by Risaliti et al. (2005a,b, 2007, 2009a,b,c) and Maiolino et al. (2010), constraints were placed upon the size of the inner disc/corona region [$R \leq 10^{14}$ cm, or $\leq$170 $r_{\rm g}$ for a black hole with $M = 4 \times 10^6\,{\rm M}_{\odot}$, the mean of the three mass estimates quoted in Risaliti et al. (2009b)], the distance of the eclipsing clouds from the black hole ($d \geq 2 \times 10^{15}$ cm, or $\geq$3400 $r_{\rm g}$) and the physical parameters of the clouds themselves ($n_{\rm c} \sim 10^{10}$–$10^{11}\,{\rm cm}^{-3}$, $v_{\rm c} \geq 1000\,{\rm km\,s}^{-1}$).

We have performed the same calculations with our data, interpreting the four dips in the X-ray light curves of the 2010 observations as eclipses in order to compare the constraints we derive on the physical parameters of the system with those of Risaliti et al. and Maiolino et al. Assuming that the inner disc extends down to the marginally stable orbit for a maximally rotating, prograde black hole ($r_{\rm in} = 1.24\,r_{\rm g}$), and estimating the average time for the onset of the eclipse to take place at $\geq$5 ks (see Fig. 1; roughly five times longer than the onset time for the eclipses in 2008), the inferred cloud velocity is $v_{\rm c} \leq 1470\,{\rm km\,s}^{-1}$. If this velocity is Keplerian, we can then calculate a distance of the clouds from the black hole of $d_{\rm c} \geq 2.5 \times 10^{16}$ cm. Assuming an average 2010 eclipse duration of $\sim$80 ks from Fig. 1 (three to four times longer than eclipses in 2008), we can place an upper limit on the size of the hard X-ray source of $r_{\rm x} \leq 1.2 \times 10^{13}$ cm. Estimating the density of the occulting clouds from the column densities in the low-flux time intervals 2010a and 2010b observations, we find that the allowed range corresponds to $n_{\rm c} = 6.5 \times 10^{10} - 1.6 \times 10^{11}\,{\rm cm}^{-3}$.

In short, the longer onsets of the eclipses in 2010 compared with those of 2008 yield cloud velocities roughly consistent with, though slightly higher than, those found in a previous work. The density of the clouds is consistent with previous results, however. The longer durations of the 2010 eclipses therefore suggest either larger or more distant clouds, in keeping with our measurements in the previous paragraph. Risaliti et al. and Maiolino et al. state that the most likely location of these clouds is the BELR ($\leq 10^{16}$ cm, or $\leq$17 000 $r_{\rm g}$). If the dips in the two 2010 light curves are indeed eclipse events, the absorbing clouds may lie on the outskirts of the BELR, or beyond, in 2010. If these are not true eclipse events with defined clouds moving into and out of the line of sight to NGC 1365, but rather represent periodic thickenings in a prolonged absorbed state, then we may see a new type of structure associated with the cold absorber in this AGN. In either case, the nature of the occulting medium has clearly changed considerably in either distance or physical structure from 2008 to 2010.

We do note that the combination of higher average column density and lower average power-law flux in the 2010 observations compared with the 2008 observation could result in the dips we observe in the 2010 X-ray light curves having less contrast from the mean than the clear eclipse events seen in 2008. Even if the same clouds from 2008 were to pass through our line of sight in 2010, the overall lower flux, state of NGC 1365 at this time would prevent us from seeing the same sharp changes in the light curves and hardness ratios seen in the 2008 data. The depth and contrast of the dips in 2010 alone are not enough to rule out a similar eclipsing cloud structure to that of 2008; rather, the duration of the dips and length of the onset of the dips are the primary indicators of a change in the size and/or location of the absorbing gas.

5.2 The nature of the inner disc/corona region

In the 2008, 2010a and 2010b *Suzaku* data, we observe the flux of the PLC changing significantly on hours- and weeks-long time-scales (Tables 2 and 3). The 2008 and 2010a observations coincidentally caught NGC 1365 with only an $\sim$10 per cent difference (1.6σ) in their average continuum strengths, but the power-law flux dropped by a factor of $\sim$2.1 (5.8σ) in the two weeks between 2010a and 2010b. The power-law strength did not change significantly during either 2010 observation, but the 2008 data do show a sudden drop by a factor of $\sim$2.0 (2.3σ) from interval #2−3, followed by a near-full recovery by interval #4.

We can then examine the flux of the inner disc reflector (RDC) during these time frames in the context of the PLC flux variation. Though the uncertainties on our measurements of the RDC flux are larger, on average, than those on the PLC flux, we stress that the RDC is nonetheless a necessary and variable component of the best-fitting model (see Section 4.1). We note the following trends (see Table 3 and Figs 8 and 9).

(i) The PLC and RDC fluxes vary significantly during 2008, though these variations appear uncorrelated. By contrast, the PLC and RDC fluxes do not vary significantly within either 2010 observation (though the RDC does decrease sharply, albeit with large error, during the last time interval of 2010b).

(ii) Though there is no evidence suggesting correlated variability within each observation, when taken together, the three observations indicate a significant anticorrelation between the PLC and RDC (see Fig. 9), with a Spearman's rank coefficient of $\rho = -0.718$ with the corresponding correlation P-value = 0.0008 using the t-distribution.

In qualitative terms, trend (ii) is consistent with the light-bending model of Miniutti & Fabian (2004) and Miniutti (2006), in which a compact corona (or a compact, active region within a larger corona) is located at some height h from the accretion disc along the spin axis of the black hole. Inverse Compton-scattered photons from this corona get reflected back down on to the surface of the underlying disc, irradiating it with X-rays from the power-law continuum. The degree of anisotropy of this radiation depends on the height of the corona, with lower heights corresponding to greater degrees of anisotropy, or light bending due to general relativity. Within the light-bending paradigm, variations in the strengths of the power law versus inner disc reflector can be attributed to variations in the height of the corona along the spin axis. A coronal height of $h \leq 4\,r_{\rm g}$ would result in the continuum and inner disc reflection component normalizations being positively correlated, and $h \geq 4\,r_{\rm g}$ would result in these variables being uncorrelated (though the quantitative values depend on geometry; e.g. Niedźwiecki & Życki 2008).

An examination of the theoretical predictions for the relation between the PLC and RDC fluxes as the intrinsic coronal luminosity changes is presented in fig. 7c of Niedźwiecki & Życki (2008). Here, the authors assume that the black hole is maximally rotating in the prograde sense with $a = 0.998$, and that the changes in PLC flux correspond to the intrinsic luminosity of the source changing with the distance of the primary emitting region of the corona from the disc surface according to radial emissivity of a Keplerian disc. This predicted RDC versus PLC flux relation bears a striking resemblance to the middle panel of our Fig. 9, depicting the observed relationship between these two variables in our spectral fitting for NGC 1365. Our data points most closely mirror the restricted region

of parameter space in the Niedźwiecki & Życki (2008) plot around the inflection point, which corresponds to a coronal distance of $h \leq 6\,r_{\rm g}$ from the disc. The similarity of our Fig. 9 to the theoretical prediction of Niedźwiecki & Życki (2008) supports our inferences of a compact corona and high black hole spin in this source, where the changes in the PLC flux are due not only to changes in the location of the emitting region(s) of the corona, but also due to changes in the intrinsic luminosity of the corona between and within our observations.

We will discuss our results within the framework of the light-bending model in greater depth in Brenneman et al. (in preparation).

5.3 Variability of the WA

A significant column of ionized absorbing gas has been observed in NGC 1365 during the majority of the X-ray pointings to date, with column densities, ionizations and outflow velocities in the range $N_{\rm H} \leq 10^{22}{-}5 \times 10^{23}\,{\rm cm}^{-2}$, $\xi \sim 3000$–$5500\,{\rm erg\,cm\,s}^{-1}$ and $v_{\rm out} \sim 1000$–$5000\,{\rm km\,s}^{-1}$, respectively. This WA manifests as the Fe XXV and Fe XXVI Kα and Kβ absorption lines from 6.7 to 8.3 keV (Risaliti et al. 2005a, 2007). Though this WA has not shown variability within observations (i.e. hours- and days-long time-scales), significant variability in column density, ionization and outflow velocity has been noted on time-scales of weeks and longer.

The three *Suzaku* observations of NGC 1365 showcase the nature of this variability. No significant changes are seen in the WA properties during 2008 (∼160 ks), 2010a (∼150 ks) or 2010b (∼300 ks), but the column density, ionization and outflow velocity all vary significantly between pointings. From the 2 years between 2008 and 2010a, $\Delta N_{\rm H}$ changed by a factor of $+1.7^{+0.3}_{-0.3}$, $\Delta\xi$ changed by a factor of $+1.8^{+0.4}_{-0.3}$, and $\Delta v_{\rm out}$ changed by a factor of $-1.9^{+1.1}_{-0.4}$. In the two weeks between 2010a and 2010b the absorption lines nearly disappear, with $\Delta N_{\rm H}$ changed by a factor of $-10.3^{+1.1}_{-4.2}$, $\Delta\xi$ changed by a factor of $-1.8^{+0.6}_{-0.5}$ and $\Delta v_{\rm out}$ changed by a factor of $+1.6^{+1.2}_{-0.9}$. Note that the increase in outflow velocity from 2010a to 2010b is within the error bars of the two parameters and is therefore not statistically significant. The reason for the lower limit on the noticeably large drop in column density between 2010a and 2010b is that the 2010b column density is at the lowest end of its parameter space in our XSTAR table model.

Assuming a lower limit of 300 ks and upper limit of ∼2 weeks for the time-scale of variability of the WA yields constraints on its distance from the source of the ionizing photons (presumed to be the corona) of $9 \times 10^{15}{-}3.6 \times 10^{16}$ cm, or ∼15 000–61 000 $r_{\rm g}$ for NGC 1365. This is based solely on light-crossing time, and assumes that the WA gas responds instantaneously to changes in the ionizing radiation source (which is almost certainly not true). The power-law continuum produced by the corona clearly varies over much shorter time-scales, so the distance to the absorbing gas must be comparatively large in order for the absorption lines not to vary on correspondingly short time-scales, provided that the physical properties of the warm absorbing gas remain constant.

We can also place limits on the distance of the absorbing gas from the hard X-ray source using the ionization and column density of the gas derived from our spectral fitting, as well as the $2{-}10$ keV luminosity of the ionizing continuum (Table 2). This method is likely more reliable than using the variability time-scale of the absorber alone, given the uncertainties and assumptions involved in that calculation. Calculating the distance of the gas using its ionization parameter yields distance estimates of 2.8–3.2×10^{15} for 2008, 1.1–1.9×10^{14} for 2010a and 2.5–3.9×10^{14} cm for 2010b, assuming that the absorber is in ionization equilibrium and that its thickness along the radial direction is roughly equal to its distance from the hard X-ray source. In other words, the absorbing gas is located in the range 185–$5400 r_{\rm g}$ in the system, consistent with a wind launched from the accretion disc (Hryniewicz & Czerny 2012).

We note that the power-law normalization stays relatively constant from 2008 to 2010a, then decreases significantly in 2010b, while the column of cold absorbing gas steadily increases from 2008 through 2010b. Neither component shows any apparent correlation with the variability of the warm absorbing gas.

5.4 Future work: mapping the inner accretion disc

Given the clear evidence for both inner accretion disc reflection signatures and a variable cold absorbing medium along our line of sight to the inner disc, NGC 1365 is one of only a few sources in which eclipses of the inner disc by clumps of the cold absorber can be used to examine the structure of the disc and the nature of its reflection features in detail. As described by Risaliti et al. (2011a), the differences between spectra from finely spaced time slices during an eclipse by a Compton-thick cloud with an eclipsed/non-eclipsed column density ratio of $N_{\rm H1}/N_{\rm H2} \geq 10$ can effectively provide a map of the flux and emissivity from isolated, progressive chords of the inner disc.

This type of accretion disc tomography can be used to trace the change in the morphology of the putative broad Fe Kα line during an eclipse, testing both its origin as a reflection signature (as opposed to an artefact of incorrectly modelled absorption, as in Miller, Turner & Reeves 2009) and whether it varies as expected within the framework of general relativity. Assuming that the eclipsing clouds rotate with Keplerian velocities in the same direction as the disc rotates, only the approaching (blueshifted) side of the disc will be occulted at the onset of the eclipse, followed by complete coverage, followed by only the receding (redshifted) side of the disc being occulted, followed by a total uncovering of the disc. The expected broad Fe Kα profile for a black hole and an inner disc in each of these scenarios is shown in Fig. 11, with its physical parameters taken from our time-averaged data for the *Suzaku* observations of NGC 1365. As discussed in Risaliti et al. (2011a), these changes in the line profile would be easily detectable even with current instruments, provided that the cold absorbing gas has sufficient column density during the eclipse compared to the uneclipsed state of the source. Future larger area X-ray telescopes would also be able to perform this experiment during Compton-thin eclipse events with less contrast than the scenario described above.

We are currently constructing a library of theoretical simulations describing the temporal and spectral variation of the broad Fe Kα line profile from the inner disc during eclipse events of varying physical properties. Once completed, this library will be adapted as a table model within XSPEC and other software packages that can be fitted to spectra and light curves during eclipse events. This model will be publicly available and will enable users to constrain the physical properties of the disc and the eclipsing gas (Brenneman et al., in preparation).

Further observations are clearly needed in order to unlock the potential of these eclipse events as probes of the inner environments of AGN. NGC 1365, in particular, has displayed part of a Compton-thick eclipse during 4 out of 13 observations with *Chandra, XMM* and *Suzaku*, most strikingly with *Chandra* in 2006, in which the source changed from Compton-thin to Compton-thick and back over the course of 4 d (Risaliti et al. 2007). Unfortunately, none

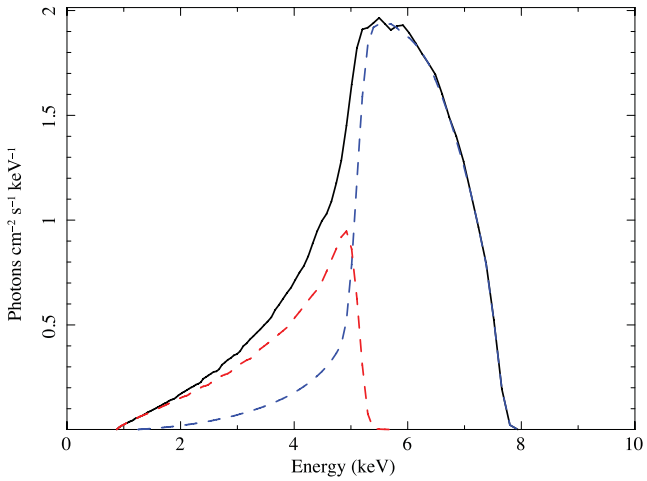

Figure 11. Expected change in the Fe Kα line profile emitted from the inner accretion disc around a black hole during an eclipse, using the parameters of NGC 1365 as described in Table 2. The solid black line shows the unocculted line profile, the blue (higher amplitude) dashed line shows the profile expected if the receding side of the disc is covered by a Compton-thick cloud and the red (lower amplitude) dashed line shows the same profile expected if the approaching side of the disc is covered.

of the observations of the source in this state was of sufficient quality to perform the type of accretion disc tomography we have discussed in this section. Our goal is ultimately to observe a full Compton-thick eclipse with enough S/N to perform a true time-resolved spectral and temporal analysis of the event with our new model. Such an analysis would be the first of its kind and would serve as an important benchmark for future variability studies of AGN with evidence for complex intrinsic absorption along the line of sight to the inner disc/corona.

6 CONCLUSIONS

We have jointly analysed three deep *Suzaku* observations of NGC 1365 dating from 2008 to 2010 in order to examine the spectral and temporal variability of the hard X-ray source, inner disc reflection and cold absorber known to eclipse the inner nucleus in this AGN. Our analysis of the broad-band X-ray spectrum from 0.7 to 40 keV and its changes over days-, weeks- and years-long time-scales has resulted in the following conclusions.

(i) The 2008 observation shows the highest flux (1.27×10^{-11} erg cm^{-2} s^{-1}) and the highest overall variability (factor of $\sim$3) of the three data sets, with the intra-observation flux and variability both decreasing through 2010a (6.13×10^{-12} erg cm^{-2} s^{-1}; factor of $\sim$1.8) and 2010b (4.05×10^{-12} erg cm^{-2} s^{-1}; factor of $\sim$1.3).

(ii) The source is at its softest in 2008, becoming harder through 2010a and 2010b, and the hardness ratio shows the most variability in 2008 as well.

(iii) Whereas the variability within each observation is dominated by the soft energies (i.e. $\leq$5 keV) in 2008, and in 2010a and 2010b the variability becomes increasingly dominated by energies above $\sim$7 keV.

(iv) The basic spectral components observed in all three data sets are a constant circumnuclear starburst, a highly ionized, outflowing WA, a clumpy cold absorber along the line of sight to the nucleus, hard X-ray emission from the corona, approximately neutral reflection from distant material in the outer disc and/or torus, and broadened, skewed reflection features from the inner disc.

(v) The spectral changes between observations are most evident in the XIS data, particularly from 2 to 6 keV (factor of $\sim$8). The PIN data also display significant variability between observations (factor of $\sim$2), though not to the degree present in the XIS data.

(vi) Incorporating both the relativistic reflection component and the cold absorber is necessary in order to adequately model the spectrum in all three epochs and flux states.

(vii) In keeping with the recent work on other type 1 AGN (e.g. NGC 3783; Brenneman et al. 2011) and the previous work on NGC 1365 (Walton et al. 2010), we find Fe/solar $= 3.5^{+0.3}_{-0.1}$. This supersolar iron abundance can readily explain the so-called hard excess noted in NGC 1365 in previous works (e.g. Risaliti et al. 2009a) without invoking an additional, ad hoc absorber partially covering the source.

(viii) While the cold absorbing column density increases by a factor of 7 from 2008 through 2010a and 2010b, the power-law normalization decreases by a factor of 2.3. Neither the distant reflection nor the relativistic reflection varies significantly between observations when taking errors into account (though some variability of the normalization of the inner disc reflector is suggested).

(ix) The broad Fe Kα line appears more prominent compared to the narrow line in 2008 and steadily less so through 2010. If this is the case, it is contrary to the behaviour of the broad iron line in, e.g. MCG-6-30-15, in which the broad line becomes significantly more prominent as the power-law flux diminishes (Fabian et al. 2002). An alternative explanation may be that the increase in cold absorbing column density from 2008 through 2010 cuts into the red wing of the broad Fe Kα line, diminishing the appearance of this feature.

(x) The WA increases by roughly a factor of 2 in column density and ionization in the 2 yr between 2008 and 2010a; simultaneously the outflow velocity drops by a factor of 2. But while the ionization drops and the outflow velocity rises again to its 2008 level in 2010b, the column density plummets by a factor of $\geq$10 in the two weeks between the 2010 observations. This variability, combined with ionization arguments, indicates that the warm absorbing gas must be located in the range $\sim$185$-$60 000 r_g from the hard X-ray source within the BELR of NGC 1365. The variability of the WA is not correlated with that of the cold absorber.

(xi) Only three spectral components appear to vary within each observation: the power law, inner disc reflector and cold absorber. The cold absorber shows the most statistically significant variations within each observation (typically $\sim$25 per cent). The power law varies comparably, though with slightly less statistical significance, and the inner disc reflector appears to vary by eye, though the errors on these measurements preclude a statistically sound interpretation of real variability within each observation.

(xii) Within the framework of the light-bending model, we use these variations in the time-resolved data to infer that the corona is compact in nature with active regions $\leq 6\,r_g$ in size.

(xiii) If we assume that the two dips in each 2010 observation of NGC 1365 correspond to eclipse events, we calculate that the eclipsing clouds must be a distance $d_c \geq 2.5 \times 10^{16}$ cm, or $\geq$44 000 r_g, from the black hole. This is an order of magnitude more distant than the eclipsing clouds in the 2008 observation. The density of the clouds remains consistent with previous observations, however. The longer eclipse durations may be due not only to the larger distance of the clouds from the hard X-ray source, but possibly to larger clouds as well.

(xiv) An observation of a full, Compton-thick eclipse with a factor of $\geq$10 change in column density could be captured with

high enough S/N and spectral resolution with current instruments to perform accretion disc tomography. Mapping the reflected X-ray emission from the disc in this way would definitively identify the origin of the putative broad iron line in NGC 1365, and would provide valuable constraints on the physical properties of the inner disc and eclipsing cloud(s).

ACKNOWLEDGMENTS

We gratefully acknowledge support from the *Suzaku* mission through NASA grant NNXlOAR44G, as well as the dedicated work of the NASA/GSFC *Suzaku* GOF team on data calibration. This work made use of archived *Suzaku* data maintained by HEASARC at NASA/GSFC. LB thanks Chris Reynolds and Mike Nowak for useful discussions that contributed to the data analysis in this paper, and Dominic Walton for providing the XSTAR grid used in this work, as well as insightful comments on the manuscript. We also thank the anonymous referee, whose critique greatly improved this work.

REFERENCES

Antonucci R., 1993, ARA&A, 31, 473
Arnaud K. A., 1996, in Jacoby G. H., Barnes J., eds, ASP Conf. Ser. Vol. 101, Astronomical Data Analysis Software and Systems V. Astron. Soc. Pac., San Francisco, p. 17
Brenneman L. W., Reynolds C. S., 2006, ApJ, 652, 1028
Brenneman L. W. et al., 2011, ApJ, 736, 103
Brenneman L. W., Elvis M., Krongold Y., Liu Y., Mathur S., 2012, ApJ, 744, 13
Chiang C.-Y., Fabian A. C., 2011, MNRAS, 414, 2345
Dauser T., Wilms J., Reynolds C. S., Brenneman L. W., 2010, MNRAS, 1460
de La Calle Pérez I. et al., 2010, A&A, 524, A50
de Vaucouleurs G., de Vaucouleurs A., Corwin H. G., Jr, Buta R. J., Paturel G., Fouqué P., 1991, Third Reference Catalogue of Bright Galaxies. Volume I: Explanations and References. Volume II: Data for Galaxies between 0^h and 12^h. Volume III: Data for Galaxies between 12^h and 24^h
Fabian A. C. et al., 2002, MNRAS, 335, L1
Fender R. P., Gallo E., Russell D., 2010, MNRAS, 406, 1425
Harrison F. A. et al., 2005, Exp. Astron., 20, 131
Hryniewicz K., Czerny B., 2012, Mem. Soc. Astron. Ital., 83, 146
Kalberla P. M. W., Burton W. B., Hartmann D., Arnal E. M., Bajaja E., Morras R., Pöppel W. G. L., 2005, A&A, 440, 775
Koyama K. et al., 2007, PASJ, 59, 23
Maiolino R. et al., 2010, A&A, 517, A47
Miller J. M., 2007, ARA&A, 45, 441
Miller L., Turner T. J., Reeves J. N., 2009, MNRAS, 399, L69
Miniutti G., 2006, Astron. Nachr., 327, 969
Miniutti G., Fabian A. C., 2004, MNRAS, 349, 1435
Miniutti G. et al., 2007, PASJ, 59, 315
Mitsuda K. et al., 2007, PASJ, 59, 1
Nandra K., O'Neill P. M., George I. M., Reeves J. N., 2007, MNRAS, 382, 194
Niedźwiecki A., Życki P. T., 2008, MNRAS, 386, 759
Patrick A. R., Reeves J. N., Lobban A. P., Porquet D., Markowitz A. G., 2011, MNRAS, 416, 2725
Reynolds C. S., Fabian A. C., 2008, ApJ, 675, 1048
Reynolds C. S., Nowak M. A., 2003, Phys. Rep., 377, 389
Reynolds C. S., Brenneman L. W., Lohfink A. M., Trippe M. L., Miller J. M., Fabian A. C., Nowak M. A., 2012, ApJ, 755, 88
Risaliti G., Elvis M., Nicastro F., 2002, ApJ, 571, 234
Risaliti G., Bianchi S., Matt G., Baldi A., Elvis M., Fabbiano G., Zezas A., 2005a, ApJ, 630, L129
Risaliti G., Elvis M., Fabbiano G., Baldi A., Zezas A., 2005b, ApJ, 623, L93
Risaliti G., Elvis M., Fabbiano G., Baldi A., Zezas A., Salvati M., 2007, ApJ, 659, L111
Risaliti G. et al., 2009a, ApJ, 705, L1
Risaliti G. et al., 2009b, ApJ, 696, 160
Risaliti G. et al., 2009c, MNRAS, 393, L1
Risaliti G., Elvis M., Bianchi S., Matt G., 2010, MNRAS, 406, L20
Risaliti G., Nardini E., Elvis M., Brenneman L., Salvati M., 2011a, MNRAS, 417, 178
Risaliti G., Nardini E., Salvati M., Elvis M., Fabbiano G., Maiolino R., Pietrini P., Torricelli-Ciamponi G., 2011b, MNRAS, 410, 1027
Ross R. R., Fabian A. C., 2005, MNRAS, 358, 211
Takahashi T. et al., 2007, PASJ, 59, 35
Tanaka Y. et al., 1995, Nat, 375, 659
Turner T. J., Miller L., Kraemer S. B., Reeves J. N., 2011, ApJ, 733, 48
Urry C. M., Padovani P., 1995, PASP, 107, 803
Uttley P., McHardy I. M., 2001, MNRAS, 323, L26
Vasudevan R. V., Fabian A. C., Gandhi P., Winter L. M., Mushotzky R. F., 2010, MNRAS, 402, 1081
Walton D. J., Reis R. C., Fabian A. C., 2010, MNRAS, 408, 601
Wang J., Fabbiano G., Elvis M., Risaliti G., Mazzarella J. M., Howell J. H., Lord S., 2009, ApJ, 694, 718

This paper has been typeset from a TEX/LATEX file prepared by the author.